Energy & Environmental Science

Hot Carrier Perovskites Solar Cell with Efficiency Exceeding 27% Enabled by Ultrafast Hot Hole Transfer with Phthalocyanines Derivatives

Journal:	*Energy & Environmental Science*
Manuscript ID	EE-ART-04-2024-001839.R1
Article Type:	Paper
Date Submitted by the Author:	23-May-2024
Complete List of Authors:	Gong, Shaokuan; Southern University of Science and Technology, Mechanical and Energy Engineering Qu, Geping; Harbin Institute of Technology, School of Chemistry and Chemical Engineering; Southern University of Science and Technology, Department of Chemistry Qiao, Ying; Southern University of Science and Technology, Chemistry Wen, Yifan; Southern University of Science and Technology Huang, Yuling; Chongqing University Cai, Siyuan; Southern University of Science and Technology Zhang, Letian; Southern University of Science and Technology Jiang, Kui; City University of Hong Kong Liu, Shang; Southern University of Science and Technology, Department of Mechanical and Energy Engineering Lin, Meng; Southern University of Science and Technology, Department of Mechanical and Energy Engineering; Beard, Matthew; National Renewable Energy Laboratory, Chemical and Nanoscience Xu, Zong Xiang; Southern University of Science and Technology, Chemistry Chen, Xihan; Southern University of Science and Technology, Mechanical and Energy Engineering

Broader context:

Hot carrier solar cells represent an attractive option for the optimal utilization of incoming solar radiation, but they are limited by the rates of hot carrier extraction. Ultrafast transient reflection spectroscopy was used measure the carrier extraction rates in perovskite-based solar cells and a correlation was derived for interfacial interaction and hot hole extraction ability. With sulfur modified phthalocyanines (Pcs) derivatives as hole transport layer (HTL), a very high hole extraction velocity was observed at high carrier density which enable a record efficiency of 27.30% at 5.9 Sun illumination for single junction perovskite solar cell. Our strategy demonstrated the potential application of high-efficiency hot carrier solar cell which might eventually break the Shockley–Queisser limit in the solar concentrator setting.

Energy & Environmental Science

PAPER

Hot Carrier Perovskites Solar Cell with Efficiency Exceeding 27% Enabled by Ultrafast Hot Hole Transfer with Phthalocyanines Derivatives

Received 00th January 20xx,
Accepted 00th January 20xx
DOI: 10.1039/x0xx00000x

Shaokuan Gong,‡[a] Geping Qu,‡[b,c] Ying Qiao,‡[b] Yifan Wen,[a] Yuling Huang,[a] Siyuan Cai,[b] Letian Zhang,[b] Kui Jiang,[d] Shang Liu,[a] Meng Lin,[a] Matthew C. Beard,[e] Zong-Xiang Xu,*[b] Xihan Chen*[a]

Hot carrier solar cells could achieve efficiencies exceeding the Shockley–Queisser limit by collecting hot carriers before they cool down. With hot-phonon bottle neck effect, hot carrier collection may be favorable at high carrier densities in concentrator photovoltaics. In this work, utilizing the excellent thermal stability of phthalocyanines (Pcs) hole transport layer (HTL), we constructed a hot hole collecting HTL. A methylthiotriphenylamine-based SMePc achieved an extraction velocity of 78900 cm/s, corresponding to a collecting distance of ~79 nm. With this HTL, an efficiency of 24.95% and certified efficiency of 24.43% are achieved under 1 Sun illumination with over 3000 hrs operational stability in N_2 (60 ℃) and over 1000 hrs at 85℃. With solar concentrator, an increase in open-circuit voltage (V_{OC}) above the theoretical cold carrier line is observed and a record efficiency of 27.30% is achieved under 5.9 Sun illumination for single junction perovskite solar cell. Our strategy demonstrated the potential application of high-efficiency hot carrier solar cell.

Introduction

In the current utility-scale photovoltaics (PV), the solar material cost has dropped to less than half of the total installation cost, which makes solar conversion efficiency crucial for deployment of PV devices and an increased power output per area could offset the cost of full PV systems. Therefore, increasing PV conversion efficiency is of vital importance. Hot carrier solar cell is a technology that could reach efficiencies beyond the Shockley–Queisser limit.[1] Hot carrier solar cells could extract carriers that have energy higher than the semiconductor bandgap thus resulting in a higher open-circuit voltage (V_{OC}) without a decrease in the photocurrent. The components of hot carrier solar cell consist of a solar absorber and energy selective contacts.[2,3] The selective contacts could extract carriers while they are hot, which could achieve higher V_{OC}. Specific molecular interactions at the selective contacts-solar absorber layer could govern the extraction efficiency. Traditional hot carrier solar cells are made with III-V semiconductors and the highest power conversion efficiency (PCE) obtained was 46% for a four-junction GaInP/GaAs/GaInAsP/GaInAs under 508 Suns irradiance.[4-6] However, due to the high cost of III-V devices, this technology is struggling to compete in the market. On the other hand, with astonishingly high efficiencies and low-cost production, perovskite-based solar cells (PSCs) have reached PCE of 26.1% certified, which is approaching the Shockley–Queisser limit for single junction near 1.5 eV bandgap.[6] Further improvements in efficiency mainly uses tandem technology which require multiple and complicated materials processing technology.[7] Hot carrier perovskite solar cells, on the other hand, could offer an easier way to achieve high efficiency. Hot carrier PSCs only consists selective contact layers and solar absorbers[8-10] such that the device structure could be vastly simplified.[11] Also, studies have shown the hot-phonon bottle neck effect in perovskites could extend hot carrier lifetime up to 100 ps at high carrier density.[12] This makes hot carrier PSCs a feasible approach under concentrated solar irradiation. Pioneer study has demonstrated the possible use of perovskites in concentrator PVs and achieved a peak efficiency of 23.6% under 14 Suns as compared to 21.1% under 1 Sun,[11] showing the feasibility of hot carrier perovskite solar cell with concentrator setting.

However, challenges still remain and one of the biggest challenges is how to efficiently extract hot carriers while they are hot. Compared with electrons, holes are harder to be extracted as effective mass of holes are generally larger and specific molecular interactions at the interfaces are closely related to the hole transport/extraction capacity.[13-19] For example, with CuSCN as hole transporting layer, an efficiency of 24.93% is achieved with 40 sun irradiation.[20] However, these studies only provide qualitative analysis on the hole extraction ability. There is a need for quantitative analyses of carrier dynamics at charge extracting interfaces and an understanding of how intermolecular interactions correlate with carrier dynamics, especially hot hole transfer dynamics which could increase the V_{OC} and allow the design of highly efficient PSCs.[12,21] Also, the HTL/perovskite

[a] Shenzhen Key Laboratory of Intelligent Robotics and Flexible Manufacturing Systems, SUSTech Energy Institute for Carbon Neutrality, Department of Mechanical and Energy Engineering, Southern University of Science and Technology, Shenzhen, Guangdong 518055, China. E-mail: chenxh@sustech.edu.cn
[b] Department of Chemistry, Southern University of Science and Technology, Shenzhen, Guangdong 518055, China. E-mail: xuzx@sustech.edu.cn
[c] School of Chemistry and Chemical Engineering, Harbin Institute of Technology, Harbin, 150001, China
[d] Department of Materials Science and Engineering, City University of Hong Kong, Kowloon, 999077, Hong Kong
[e] National Renewable Energy Laboratory, Golden, CO, 80401, United States
Electronic Supplementary Information (ESI) available: [details of any supplementary information available should be included here]. See DOI: 10.1039/x0xx00000x
‡ These authors contributed equally.

interfaces determine both the thermal stability and long-term stability of the corresponding devices. Compared with the currently commercial 2,2',7,7'-tetrakis-(N,N-di-p-methoxyphenylamine)-9,9' spirobifluorene (Spiro-OMeTAD) which requires hygroscopic dopants to ensure conductivity and are detrimental to the long-term stability.[22] Therefore, developing dopant-free HTMs is crucial for achieving efficient and stable PSCs, and it remains a significant challenge. [23,24] To date, only a few dopant-free HTMs have been reported to achieve a PCE higher than 24%.[25-29] Phthalocyanines (Pcs) possess a large-conjugated framework, excellent thermal stability, superior physical and chemical durability, affordability, and can be designed to have a tunable energy band, good carrier mobility, solubility in common solvents, and facile synthesis.[30-33] These characteristics make them a promising candidate for use as a robust HTM in perovskite solar cells (PSCs). Our result ranks among the highest reported PCE achievements, which is approaching 25%. And the Pcs HTM demonstrated the most excellent thermal stability. In addition, the side chain and central ring can be easily tuned with different substituents and metal ions, which can regulate intermolecular interactions between the Pcs and the perovskite active layer, making them a model system for hot carrier solar cells.[34]

In this work, we utilized transient absorption and reflection spectroscopy to quantitatively understand hot hole extraction through hole extraction velocity and designed a series of copper-based Pcs HTLs with sulphur side chains. The hole extraction velocity was found to increase as the carrier concentration increases. Comparing with Spiro-OMeTAD whose hole extraction velocity of maximum 4400 cm/s obtained from transient spectroscopy study, a methylthiotriphenylamine group-based SMePc reached a maximum velocity of 78900 cm/s. Such a phenomenon is an indication of semi-selective contact layer where hot holes transfer faster than band-edge holes. This high extraction velocity contributed to a 24.95% recorded efficiency (certified PCE of 24.43%) for optimized perovskite composition for FA rich (CsRbMAFA) perovskites, ranking among the highest for dopant free transport layer-based PSCs. Under concentrated Sun irradiation where hot-phonon bottle neck effect plays, a record efficiency of 27.30% is achieved under 5.9 Suns irradiation, highest for perovskite based hot carrier solar cell. Grazing incident X-ray diffraction (GIXRD), X-ray photoelectron spectroscopy (XPS), and density functional theory (DFT) calculations revealed that interactions between the S atoms of the modified Pcs and Pb of the perovskite layer provided orbital overlap for holes to efficiently tunnel through. These results could further provide guidance for the design of perovskite based hot-carrier solar cells.

Results

The structures of the Pcs derivatives used as dopant-free HTLs in an n-i-p planar PSCs are shown in Fig. 1A, they are pristine Pc, Me_2Pc, SBuPc and SMePc. Copper based Pcs are low cost and easy to synthesize with excellent thermal stability.[35] Except for the pristine Pc, the Me_2Pc is with alkyl chain and the other two Pcs are tuned with sulphur containing side chains (SBuPc and SMePc). Alkyl chains interact with perovskites primarily through van der waals interaction while sulphur might have coordination interactions. The synthetic details as well as the materials characterizations were described in Supporting Information (Scheme S1, Fig. S1-S3). Cross-sectional scanning electron microscope (SEM) imaging, Energy dispersive X-ray (EDS) mapping, X-ray diffraction (XRD), ultraviolet-visible (UV-vis) spectroscopy, ultraviolet photoelectron spectroscopy (UPS), and X-ray photoelectron spectroscopy (XPS) results from the fabricated perovskite/HTL layers are shown in Fig. S4 to S8. The SEM, EDS and XRD results show that the structure of the perovskite layer was unchanged and the HTL coverage was uniform, meaning that transient spectroscopic investigations could be applied to specifically study the influence of the Pcs HTL.

Both pure $MAPbI_3$ (MA = methyl-ammonium) and pure $FAPbI_3$ (FA = Formamidinium)-based films were investigated with half device structure (indium tin oxide (ITO)/PVK/HTL) by transient reflection (TR) spectroscopy, providing information about the extraction of carriers.[36-39] Bulk carrier dynamics were investigated with transient absorption (TA) spectroscopy (Fig. S9) and the kinetics showed bulk recombination does not affect surface carrier dynamics within the ultrafast time scale. The TR kinetics of four Pcs HTLs are shown in Fig. 1B-E. By simultaneously modelling the decay profiles includes both diffusion and surface extraction, the best fit values of the diffusion coefficient (D) and surface recombination velocity/ surface extraction velocity (SRV/SEV) values were obtained:

$$\frac{\partial N(x,t)}{\partial t} = D\frac{\partial^2 N(x,t)}{\partial x^2} - \frac{N(x,t)}{\tau_B} \quad (1)$$

$$\frac{\partial N(x,t)}{\partial x}|_{x=0} = \frac{SEV_F}{D}N(0,t) \quad (2)$$

$$\frac{\partial N(x,t)}{\partial x}|_{x=L} = -\frac{SRV_B}{D}N(L,t) \quad (3)$$

where N(x,t) is the carrier density as a function of depth (x) and time (t), D is the ambipolar diffusion coefficient and τ_B is the bulk carrier lifetime. Generally, in a metal-halide perovskite absorber layer, τ_B is of the order of hundreds of ns and can be neglected. The boundary conditions were determined such that the front surface extraction will dominate (SEV_F) and back surface recombination occurs with SRV_B. L is the thickness of the film. The initial carrier concentration is defined as:

$$N(x,0) = N_0 e^{-\alpha x} \quad (4)$$

where α is the absorption coefficient of perovskites at the excitation energy. When the HTL was not added, there will be no surface hole extraction and the carrier concentration in the perovskite film will decrease because of intrinsic surface recombination occurring at the front and back surfaces, and this can be considered to

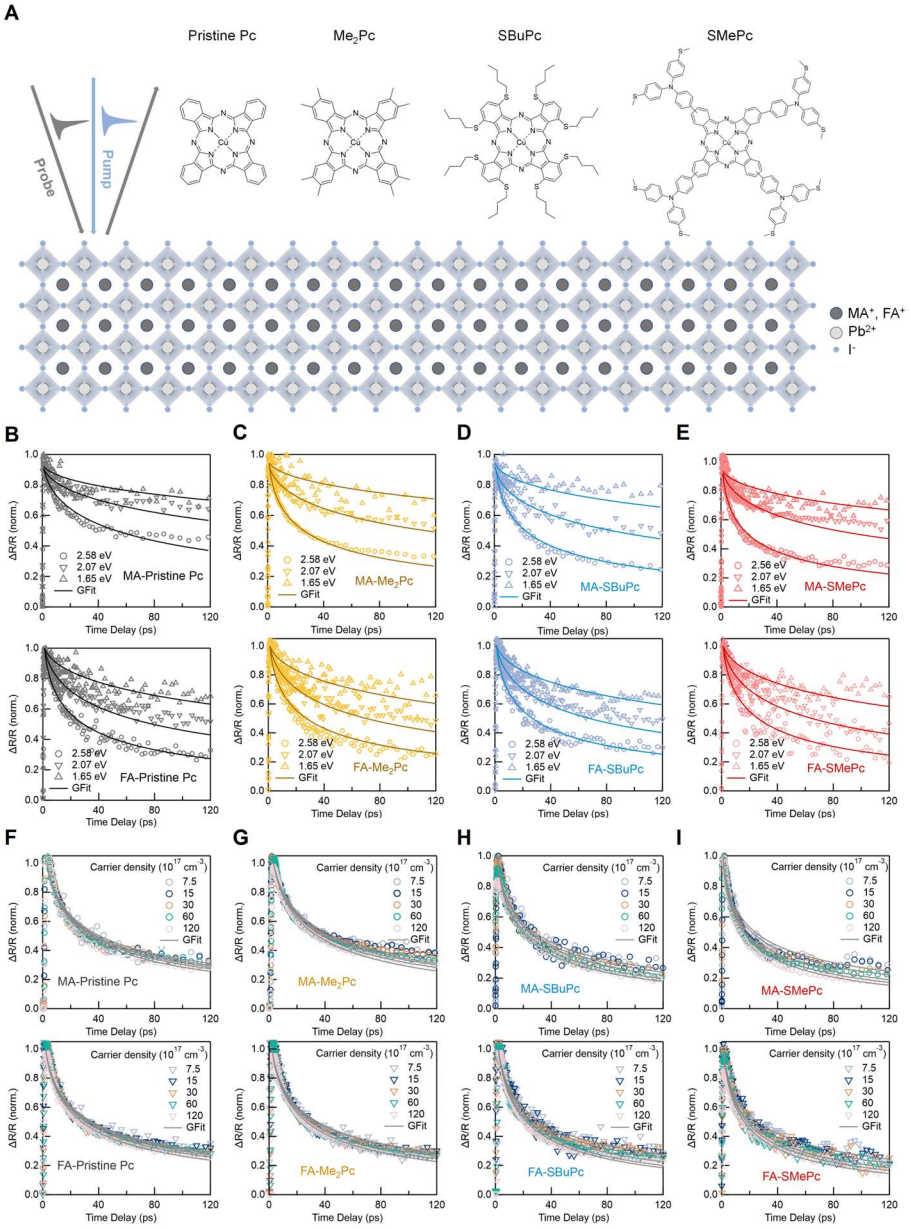

Fig. 1 Chemical structures of organic HTL molecules, schematic diagram of the experimental setup, TR spectroscopy kinetics. (A) Chemical structures of the four copper based phthalocyanines (Pcs) molecules, namely Pristine Pc, Me_2Pc, SBuPc and SMePc and schematic illustration of the interaction configuration revealed by ultrafast pump-probe measurements. (B-E) Surface carrier kinetics from excitation at 2.58, 2.07, and 1.65 eV probed by TR spectroscopy and fitted with a diffusion-surface extraction model for MA and FA based perovskites with pristine Pc (B), Me_2Pc (C), SBuPc (D), and SMePc (E)HTLs. (F-I) TR kinetics under various carrier densities excited at 2.58 eV pump energy, modelled with *SEV* for MA and FA based perovskites with pristine Pc (F), Me_2Pc (G), SBuPc (H), and SMePc (I).

the *SRV*. Also, in the literature, the electron mobility in perovskites could be 10 times larger than the holes,[37,40] therefore, the ambipolar diffusion will be mainly limited by holes.

For the MA-based devices, the extracted *D* value was 1.5 ± 0.2 cm^2/s, and the *SRV* value was 800 ± 400 cm/s, determined as the intrinsic *SRV* on the perovskite surfaces of other samples that were not in contact with the HTL (Fig. S10). For the structure based on traditional Spiro-OMeTAD, the extracted *SEV* value (1500 ± 200 cm/s) was slightly greater than, but similar to the *SRV* of pure perovskite, indicating that the hole extraction of Spiro-OMeTAD competes with intrinsic surface recombination (Fig. S10). Conversely, the films based on copper Pcs and its derivatives exhibited *SEV* values up to 7 times as high as that of the reference Spiro-OMeTAD sample. The sample containing SMePc gave the best performance with an *SEV* value of 19300 ± 2600 cm/s which is 13 times to the reference sample (Table S1). For FA based devices, the trend stays where S containing compounds gives the best *SEV* value of 21900 ± 1500 cm/s. (Table S2)

The hot carrier effect is most obvious at high carrier density and above band gap excitation; therefore, we extend the TR spectroscopy at higher carrier density to understand hot carrier extraction effect. The perovskites were excited with high energy photons (2.58 eV)

above the perovskite bandgap to provide excess energy for carriers. As shown in Fig. S11, all the TA spectra showed a high energy tail spanning from 600 to 700 nm, corresponding to a hot-carrier distribution that is initially generated inside the perovskite film.[12] Fig. 1F-I represent the TR kinetics (See Fig. S12 for TA dynamics) with various pump fluences for both MA and FA based devices. The extracted *SEV* values are shown in Table S3-4. For both MA and FA devices, the *SEV* of all the HTLs was higher at higher carrier density, indicating that hole extraction increases at higher carrier densities. With increasing carrier density, the hot-phonon bottleneck effect can slow down the cooling rate of hot carriers up to hundreds of ps, allowing for hot carriers to be harvested by HTLs.[12,41,42] Notably, for MA based devices, when comparing the different HTLs, for Spiro-OMeTAD, the *SEV* remained essentially unchanged at various pump fluences (Fig. S13), reaching only 2650 ± 400 cm/s at a carrier density of 1.2×10^{19} cm^{-3}, which is only 1.8 times as high as the *SEV* at a low carrier density of 7.5×10^{17} cm^{-3}. However, on increasing the carrier density from 7.5×10^{17} cm^{-3} to 1.2×10^{19} cm^{-3} in systems with the pristine Pc and Me_2Pc HTLs, the *SEV* more than doubled (Fig. 1F-G, Table S3-4). The largest increase in *SEV* was observed for SBuPc and SMePc, for which the *SEV* was nearly 4 times as high at a high carrier density than a low carrier density (Fig. 1H-I, Table S3-4). For FA based devices, SMePc molecules also have the strongest hole extraction ability with an *SEV* of 21900 ± 2600 cm/s at low carrier

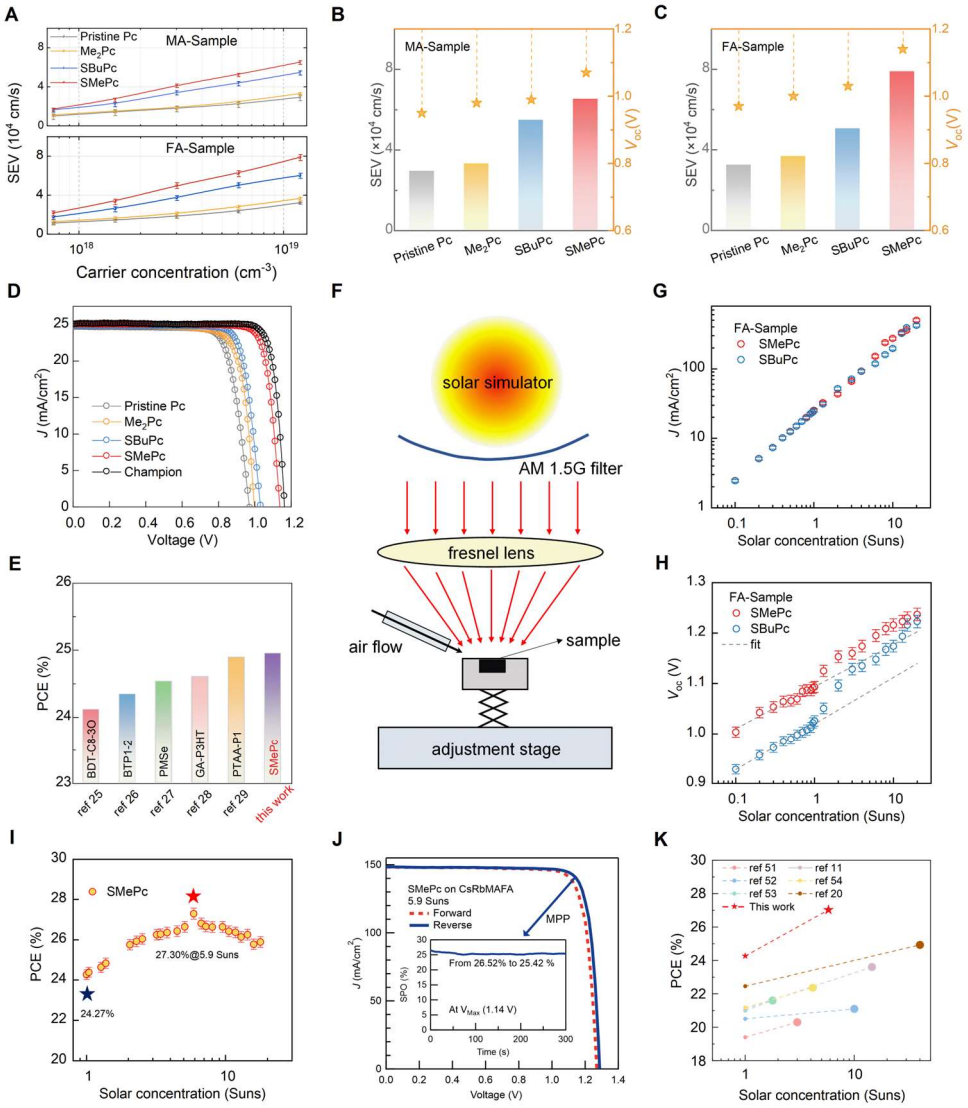

Fig. 2 *SEV*, V_{OC} and concentrator device performance. (A) Distribution of *SEV* values at different carrier densities for both MA- and FA-based samples with four Pcs molecules. (B and C) Distribution of SEV values at high carrier density (1.2×10^{19} cm^{-3}) and V_{OC} values for both MA- (B) and FA- (C) based samples with four Pcs molecules. (D) J-V curves characteristic of FA-based PSCs and champion sample of CsRbMAFA perovskite with SMePc. (E) Summary of the published results of high-performance dopant-free organic hole transport materials-based PSCs.[25-29] (F) Schematic diagram of the concentrator setup when a Fresnel lens was used to concentrate sun light from a solar simulator. (G and H) J_{SC} (F) and V_{OC} (G) of FA-based perovskites with SBuPc and SMePc as HTL. Current density increased linearly with irradiation (Solar concentration), where the V_{OC} increases deviates from the theoretical log line. (I and J) Concentrator solar cell performance of FA rich (CsRbMAFA) perovskite with SMePc as HTL. (K) Summary of the published results of concentrator performance of PSCs.[11,20,51-54]

concentration and the *SEV* for hot carriers was as high as 78900 ± 3100 cm/s at high initial carrier concentrations (1.2×10^{19} cm^{-3}), which is approximately 1% of the hole thermal velocity (by taking $v_{th} = \sqrt{\frac{3kT}{m^*}}$), indicating quasi-ballistic transfer of holes.[43-45] This very fast hole transfer process might also correlate with the long-range hot carrier transport that is observed in halide perovskites.[46,47] A carrier density dependent experiment with excitation at 1.65 eV did not show any hot carrier effect (Fig. S14).

Fig. 2A-C show the obtained *SEV* compared with V_{OC} for MA- and FA-based perovskites. Clearly, the *SEV* values corresponded well with the V_{OC} values. In addition, Fig. 2D, Table S5-6 and Fig. S15-16 show the performance of corresponding devices based on the four types of Pcs HTL. For MA based devices, the observed V_{OC} increase from 0.94 V for pristine Pc to 1.07 V for SMePc. For FA based devices, the observed V_{OC} was 0.97 V for pristine Pc and 1.14 V for SMePc, which reflects a >17% increase. The device with SMePc had the best power conversion efficiency of 23.59% with FA-based perovskites and the champion efficiency of 24.95% with FA rich (CsRbMAFA) perovskites over 3000 hrs stability (60°C) and over 1000 hrs at 85°C with MPP tracking, which is the highest reported performance of a dopant-free Pcs-based PSCs (Fig. 2E, Fig. S17, Table S7) and certified PCE of 24.43% (Fig. S18). A larger *SEV* reflects a better hole extraction ability. Thus, the excellent hole extraction ability observed for the sulphur side chain indicates that S-perovskite interactions promote the hole extraction. In addition, the *SEV* values of the different HTLs correlated with the photovoltaic performance characteristics of their corresponding devices. The charge extraction ability is related to the V_{OC} and fill factor (*FF*),[48,49] whereas the short-circuit current density (J_{SC}) remained nearly unchanged. This indicates that the sulphur side chain HTLs more effectively extracted charges, including hot carriers, which resulted in a large increase in the V_{OC}.

To further understand the hot carrier transfer of different HTLs, we performed a concentrated solar cell. Because SBuPc and SMePc give the best performance, we focused on these two configurations. Fig. 2F shows the concentrator setup where a Fresnel lens was used to concentrate sun light from the solar simulator. Cold air gas was constantly blown into the cell to avoid overheating due to thermal effects. Fig. 2G-H shows the V_{OC} and J_{SC} for the corresponding devices. (See I-V curves in Fig. S19-S20). For the V_{OC}, the value was plotted against the log of the number of Sun intensity, because the V_{OC} should have a linear relationship with the log of carrier density.[50] According to Shockley–Queisser theory, the V_{OC} is proportional to the quasi-Fermi-level splitting because the carriers are assumed to relax to the band-edge position, according to:

$$V_{OC} = E_f^n - E_f^p = k_b T ln \frac{\Delta n \Delta p}{N_C N_V} + E_g \qquad (5)$$

Where k_b is the Boltzmann constant, $\Delta n \Delta p$ is the excited carrier density of electrons and holes, $N_C N_V$ are the density of states near conduction and valence band and E_g is the bandgap. Therefore, the V_{OC} is proportional to the log of carrier density (number of Suns). However, J_{SC} should be proportional to the carrier density, and this is indeed the case for SBuPc- and SMePc-based devices, as shown in Fig. 2G. In terms of the trend for V_{OC}, at a low carrier density (below 2 Sun), the slope of V_{OC} vs Sun number is linear as indicated by the dashed line and consistent with band-edge carrier behaviour, as suggested by equation 5. However, when more carriers are injected above a 2-Sun carrier density, the V_{OC} increases above the theoretical limit (indicated by the dotted line) for both SBuPc- and SMePc-based devices. This is an indication that hot carrier transfer occurs at a higher carrier density because hot carriers can increase the quasi-Fermi-level splitting and lift the V_{OC}. The best performing concentrator devices with FA rich (CsRbMAFA) composition gives 1.355 V V_{OC} under 17.8 Suns compared to 1.148 V under 1 Sun as shown in Fig. S21, indicating the enormous potential of hot carrier extraction contributing to the improvement of V_{OC}. At the same time, the corresponding PCE achieved a 27.30% efficiency under 5.9 Suns and the corresponding stabilized power output (SPO) data is determined by holding the cell at a fixed voltage near the maximum power point on the J–V curve for 300 s as shown in Fig. 2I-J, (See Fig. S21) well over the current certified efficiency of 26.1% and it is the highest efficiency for concentrator perovskite-based PV. (Fig. 2K and Table S8) [11,20,51-54] At higher light intensity, a decrease in efficiency is observed which might be a result of excess heating and increased hysteresis effect[11]. Another interesting point here is that *SEV* values are higher with high carrier density, which suggests that the S containing HTLs could extract hot carriers faster than cold carriers.

To study the influence of the side chain of the Pcs molecules and its effects on the hole transport efficiency, we examined the molecular binding configuration and arrangements of the four Pcs HTLs on an FA perovskite layer. For example, XPS has been shown to provide surface binding configuration,[55] and our XPS data are shown in Fig. 3A-D, Fig. S22 and Fig. S23. Especially the XPS data (Fig. 3A-D) are detected by a 10-degree incident angle which could provide molecular binding energy information with a ~1.7 nm depth. We can see that four Pcs samples all showed clear Cu 2p peaks, and SBuPc and SMePc also showed Cu satellite peaks near 944 and 970 eV. The satellite peaks show an increase in binding energy, which suggests a deshield in Cu bonding environment[56]. Because the Pcs molecules are π-conjugated, therefore, the π-π stacking of the Pcs might be similar. The existence of satellite peaks of Cu could suggest that SBuPc and SMePc have more Cu exposed to an open environment, possibly to the perovskite surfaces. Also, we performed SEM study to understand the surface roughness and the SEM images of the Pcs molecules on perovskite in Fig. S4 showed that the surface of pristine Pc and Me_2Pc films are relatively rough which will influence the contact between HTL and metal electrode.[36] The SEM images for SBuPc and SMePc show less surface roughness and therefore better contact for electrodes. Furthermore, the (Energy dispersive spectroscopy) EDS line sweep mode was used to analyse the elemental contents of the Pcs-containing films. As shown in Fig. 3E-H, among the four Pcs molecules, the intensity of Cu from the four Pcs HTLs on the perovskite was similar and the element content of all samples was almost unchanged at different locations, indicating that the Cu content over the entire Pcs film was similar and four Pcs molecules were distributed evenly on the perovskite, owing to the high penetration of the EDS measurement.

To quantitatively understand the interfacial molecular interactions and correlate with the molecular arrangement, we

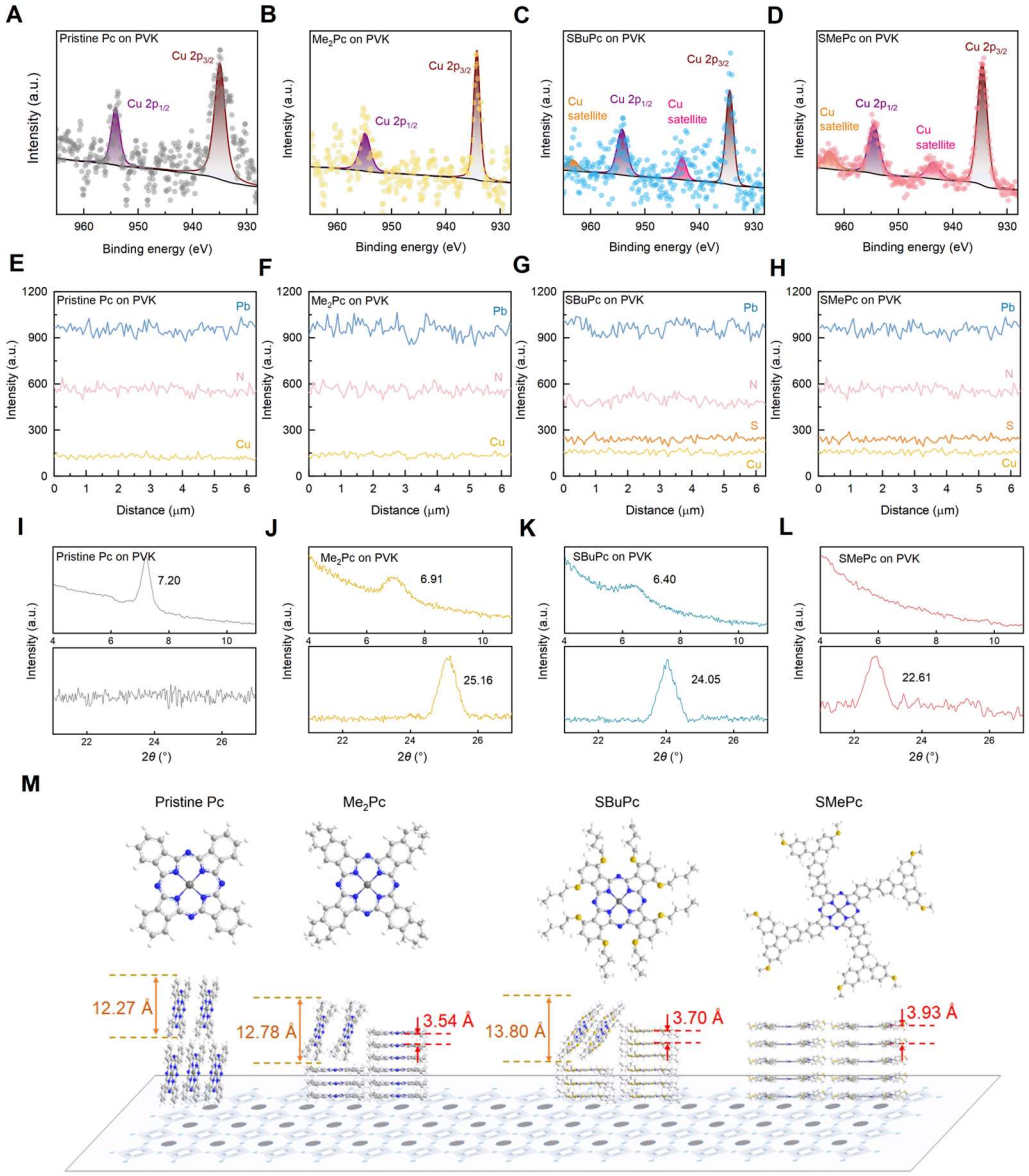

Fig. 3 Molecular binding energy configuration and arrangement of Pcs molecules for FA-based perovskites. (A-D) XPS spectra of Cu 2p for the four Pcs films with pristine Pc (A), Me_2Pc (B), SBuPc (C) and SMePc (D) on FA-based perovskite substrate. (E-H) Linear scanning mode of EDS data with different elements under SEM performance for the four Pcs films with pristine Pc (E), Me_2Pc (F), SBuPc (G) and SMePc (H) on FA-based perovskite substrate. (I-L) GIXRD patterns of four Pcs films with pristine Pc (I), Me_2Pc (J), SBuPc (K) and SMePc (L) on FA-based perovskite substrate. (M) Illustration of the molecular arrangement of four Pcs films on perovskite substrate.

performed XRD analysis of the films. The results shown in Fig. S6 indicate that there was no change in the crystal structure. GIXRD was also performed and are shown in Fig. 3I-L. The diffraction signal is at 7.20°, 6.91°, and 6.40°, respectively, corresponding to inter-planar distances of 12.27 Å for pristine Pc, 12.78 Å for Me_2Pc, and 13.80 Å for SBuPc, consistent with estimated molecular length from DFTs calculation (Fig. S24, S25). This result suggests a nearly perpendicular orientation of the pristine Pc with respect to the perovskite (i.e., edge-on adsorption).[57,58] Notably, no diffraction signal was observed for SMePc at small angle below 8°. Such an absence of the peaks is not due to changes in background as the same background fitting is applied to all Pcs (Fig. S6). In the meantime, GIXRD data at higher angle presents second diffraction signal from 22° to 26°. Such an appearance of peaks correlates with a gradual disappearance of peaks in the low angle region. Such a change can be related to a face-on molecular orientation of Pcs as suggested by the literature[59], which maximizes the surface-complex contact and likely contributes to the improved hole mobility of the HTL. Therefore, we believe that the pristine Pc sample had an edge-on arrangement, the SMePc sample had a face-on arrangement, and the other two samples (Me_2Pc and SBuPc) had a mixture of molecular arrangements, which reveals the strength of the interfacial interactions. (Fig. 3M)

To further analyse the interaction configuration at the interface, XPS and UPS were used to analyse the Pcs molecules separately when deposited on perovskite films. The peak fitting results (Fig. 4A-D) showed that the Pcs HTL and perovskite layers had a peak from a S-

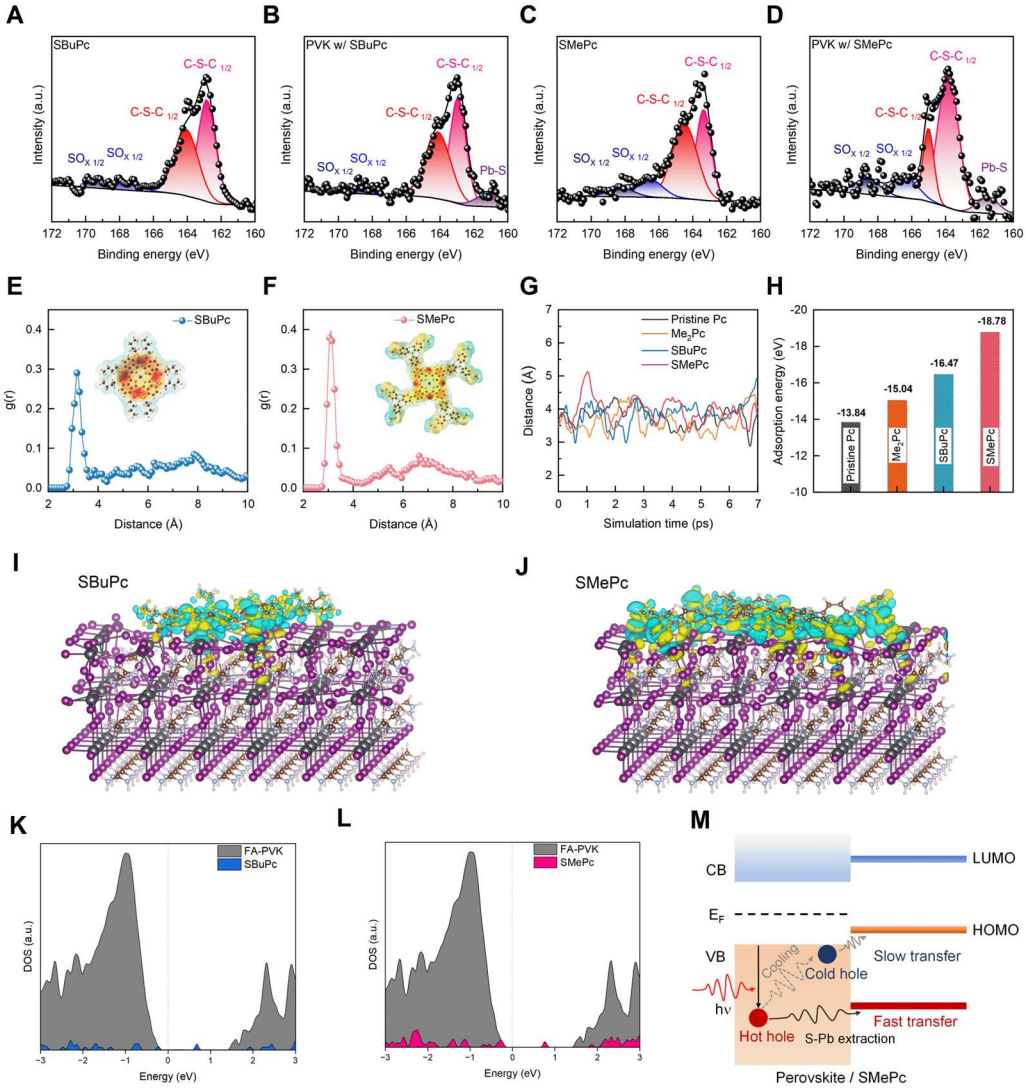

Fig. 4 Interfacial configuration of the Pcs molecules. (A-D) XPS data and peak fitting for SBuPc (A and B) and SMePc (C and D) HTLs alone and deposited on the perovskite. (E and F) Radial distribution functions (RDFs) between the S atoms in the SBuPc (E) and SMePc (F) molecules and the Pb atoms on the perovskite surface. (G) Evolution of Cu-I bond distance versus simulation time during AIMD simulations at 300 K. (H) Histogram of adsorption energies between the four Pcs molecules and perovskite. (I and J) Charge density differences between the SBuPc (I) and SMePc (J) molecules and the three-layer $FAPbI_3$ perovskite. Electron depletion/accumulation is depicted by the blue/yellow, isosurfaces at ±0.004 |e| $Å^{-3}$. (K and L) Total density of states (DOS) for the FA-based perovskites with the (K) SBuPc and (L) SMePc molecules. (M) Illustration of hole transfer through interfacial S-Pb interactions. Added in hot carrier extraction speed faster than cold carriers. Molecular levels instead of bands.

Pb interaction at a binding energy of ~161 eV and the S-Pb interaction is possibly a coordination interaction. Thus, the perovskite can form S-Pb coordination interactions with SBuPc and SMePc, i.e., the two molecules that contained sulphur. The estimated contact area of the SMePc molecule es (8.9%) is larger than that of SBuPc (8.5%) (Table S9), which is related to the fact that the hole extraction rate of SMePc is higher than that of SBuPc. Steady-state photoluminescence (PL) and time-resolved photoluminescence (TRPL) spectra were also measured, as shown in Fig. S26 and Fig. S27 and the fitted lifetimes are shown in Table S10. The sample with SMePc exhibited the fastest carrier extraction, as indicated by the quenching of PL intensity and the short PL lifetime. The radial distribution functions of the S atoms and Pb atoms are shown in Fig. 4E-F. Among them, SMePc exhibited the closest proximity to the perovskite surface with the Cu-I distances unchanged (Fig. 4G), suggesting that the primary interaction occurs through S-Pb coordination interactions which also contributes to the highest adsorption energies (Fig. 4H, Table S12).

Discussion

The face-on geometry of these molecules, as confirmed by XPS and GIXRD characterization suggests that a planar interaction of Pcs with the perovskite surface favours charge extraction. Previous studies have indicated that S-Pb bonds induce an additional back-surface field, which might improve device V_{OC}.[55] In our case, the Pcs layer is undoped such that S-Pb coordination interactions may not directly

induce a field. In donor-acceptor systems, charge transfer is best described by Fermi's golden rule or Marcus theory,[60,61] where the rate of charge transfer depends on a key integral:

$$k \sim \frac{2\pi}{\hbar} < f|H|i >^2 \rho(E_{fi}) \qquad (6)$$

where the first term represents the overlap between the initial donor and the final acceptor states and $\rho(E_{fi})$ represents the density of states of the acceptor. And to further understand the effect of hot carrier extraction, we conducted the charge density differences and density of states (DOS) calculations between the Pcs molecules and the perovskite in Fig. 4I-J. Interestingly, with both SBuPc and SMePc as HTL, the charge density is highly concentrated between Pb and S, indicating a potential bond formation. Also, in the DOS, both SBuPc and SMePc show orbital overlap with the perovskite in the valance band. For SMePc, there is even a larger orbital overlap ranging from 1 eV to 2 eV below the valance band edge (Fig. 4K-L), such a channel could enhance the final $\rho(E_{fi})$ term and significantly increase the probability of the hot carrier transfer, resulting in much higher hot carrier tunnelling rate that increase the *SEV*, which results in a V_{OC} increase. Fig. 4M illustrate the effect of hot carrier transfer where hot holes could tunnel through the barrier and be extracted out with higher energy. In the TR experiment, the pump used is 2.58 eV, which is close to 1 eV above the bandgap, thus, carriers with 1 eV excess energy could tunnel through the DOS overlap and resulting in a large surface extraction velocity. Cold carriers at band edge may not have this large overlap that could be extracted slower.

Remarkably, at a high charge carrier density, due to the hot-phonon bottle neck effect, the hot carrier in perovskites takes longer to relax, resulting in a hotter carrier distribution. For example, for $MAPbI_3$ based perovskites, the hot carrier lifetime could reach ~100 ps above 10^{18} cm^{-3} carrier density, allowing sufficient time for carrier extraction.[12] With S-Pb interactions, hotter carrier could be extracted before they reach band edge and thus greatly enhances the V_{OC} of the corresponding devices. With 78900 cm/s hole extraction velocity, the hot carrier's extraction distance could reach near 78.9 nm taking ~100 ps relaxation time. Based on the general absorption coefficient α for perovskites,[62] 78.9 nm correspond to penetration depth of light with energy above 2.58 eV. Thus, high energy carriers that are generated with energy above 2.58 eV could be efficiently collected by the S-Pb bond and achieve over 27% efficiency in concentrator setting.

Conclusion

In our study, we designed phthalocyanines (Pcs) based hot hole collecting layer. With methylthiotriphenylamine-based SMePc, we achieved an extraction velocity of 78900 cm/s, corresponding to a hot hole collecting distance of ~79 nm. With this HTL, an efficiency of 24.95% and certified efficiency of 24.43% are achieved under 1 Sun illumination with over 3000 hrs operational stability for FA rich perovskites. With solar concentrator, an increase in open-circuit voltage above the theoretical cold carrier line is observed and a record efficiency of 27.30% is achieved under 5.9 Sun illumination for single junction perovskite solar cell. Grazing incident X-ray diffraction (GIXRD), X-ray photoelectron spectroscopy (XPS), and density functional theory (DFT) calculations revealed that interactions between the S atoms of the modified Pcs and Pb of the perovskite layer provided orbital overlap for holes to efficiently tunnel through. Our strategy demonstrated the potential application of high-efficiency hot carrier solar cell.

Author Contributions

S. G., G. Q., and Y. Q. conceived the idea, designed and conducted the experiments, and prepared the manuscript under the supervision of Z. X. X and X. C.. Y. W., Y. H., S. L., M. L. and M. C. B. assisted with the spectroscopy and concentrator measurements. S.C. synthesized and characterized phthalocyanine molecules. K. J. is responsible for perovskite solar cell packaging. Y. Q. performed the DFT calculations. G. Q. performed GIXRD characterization under the supervision of Z. X. X. All authors discussed the results and commented on the manuscript.

Conflicts of interest

There are no conflicts to declare.

Acknowledgements

This work is supported by the Natural Science Foundation of Guangdong Province under contract number 2023A1515011145, Guangdong Major Project of Basic and Applied Basic Research (2023B0303000002), Guangdong Provincial University Science and Technology Program (Grant No. 2023KTSCX119) and Shenzhen Science and Technology Innovation Commission under contract number JCYJ20220530114809022 and ZDSYS20220527171403009. Z.-X. Xu acknowledge the support from the National Natural Science Foundation of China (No. 21975116), the Major Program of Guangdong Basic and Applied Research (Nos. 2019B121205001 and 2019B030302009), and Shenzhen-Hong Kong-Macau Science and Technology Plan C (No. SGDX20210823104205034). M.C.B acknowledges support as part of the Center for Hybrid Organic Inorganic Semiconductor for Energy (CHOISE) an Energy Frontier Research Center funded by the Office of Basic Energy Sciences, Office of Science within the U.S. Department of Energy. This work was partially authored by the Alliance for Sustainable Energy, LLC, the manager and operator of the National Renewable Energy Laboratory for DOE under contract number DE-AC36-08GO28308. The views expressed in the Article do not necessarily represent the views of the DOE or the U.S. Government. The U.S. Government retains and the publisher, by accepting the article for publication, acknowledges that the U.S. Government retains a nonexclusive, paid-up, irrevocable, worldwide license to publish or reproduce the published form of this work, or allow others to do so, for U.S. Government purposes. We thank Daozeng Wang and Prof. Longbin Qiu for assistance with concentrator experiments.

References

1 Ross, R.T. and Nozik, A.J., *J. Appl. Phys*, 1982, **53**, 3813-3818.
2 Nozik, A. J., *Nat. Energy*, 2018, **3**, 170-171.
3 Conibeer, G.J.,Jiang, C.W., König, D., Shrestha, S., Walsh, T. and Green, M.A., *Thin Solid Films*, 2008, **516**, 6968-6973.
4 Nguyen, D.T., Lombez, L., Gibelli, F., Richard, S.B., Corre, A.L., Durand, O.D. and Guillemoles, J.F., *Nat. Energy*, 2018, **3**, 236-242.
5 Esmaielpour, H., Dorman, K.R., Ferry, D.K., Mishima, T.D., Santos, M.B., Whiteside, V.R. and Sellers, L.R., *Nat. Energy*, 2020, **5**, 336-343.
6 Fano, U., *Phys. Rev.*, 1961, **124**, 1866-1878.
7 Zheng, J., Duan, W., Guo, Y., Zhao, Z.C., Yi, H., Ma, F.J., Caro, L.G., Yi, C., Bing, J., Tang, S., et al., *Energy Environ. Sci.*, 2023, **16**, 1223-1233.
8 Li, N., Niu, X., Chen, Q. and Zhou, H., *Chem. Soc. Rev.*, 2020, **49**, 8235-8286.
9 Rajagopal, A., Yao, K. and Jen, A. K. Y., *Adv. Mater.*, 2018, **30**, 1800455.
10 Peng, W., Mao, K., Cai, F., Meng, H., Zhu, Z., Li, T., Yuan, S., Xu, Z., Feng, X., Xu, J., et al., *Science*, 2023, **379**, 683-690.
11 Wang, Z., Lin, Q., Wenger, B., Christoforo, M.G., Lin, Y.H., Klug, M.T., Johnston, M.B., Herz, L.M. and Snaith, H.J., *Nat. Energy*, 2018, **3**, 855-861.
12 Yang, Y., Ostrowski, D.P., France, R.M., Zhu, K., Lafemaat, J.V.D., Luther, J.M. and Beard, M.C., *Nat. Photonics*, 2016, **10**, 53-59.
13 Yao, Y., Cheng, C., Zhang, C., Hu, H., Wang, K. and Wolf, S.D., *Adv. Mater.*, 2022, **34**, 2203794.
14 Jeon, N.J., Na, H., Jung, E.H., Yang, T.Y., Lee, Y.G., Kim, G., Shin, H.W., Seok, S.I., Lee, J. and Seo, J., *Nat. Energy*, 2018, **3**, 682-689.
15 Saliba, M., Orlandi, S., Matsui, T., Aghazada, S., Cavazzini, M., Baena, J.P.C., Gao, P., Scopelliti, R., Mosconi, E., Dahmen, K.H., et al., *Nat. Energy*, 2016, **1**, 15017.
16 Kim, G.W., Choi, H., Kim, M., Lee, J., Son, S.Y. and Park, T., *Adv. Energy Mater.*, 2020, **10**, 1903403.
17 Nazir, G., Lee, S.Y., Lee, J.H., Rehman, A., Lee, J.K., Seok, S.I. and Park, S.J., *Adv. Mater.*, 2022, **34**, 2204380.
18 Abdi-Jalebi, M., Dar, M.I., Senanayak, S.P., Sadhanala, A., Andaji-Garmaroudi, Z., Pazos-Outon, L.M., Richter, J.M., Pearson, A.J., Sirringhaus, H. and Grätzel, M., *Sci. Adv.*, 2019, **5**, eaav2012.
19 Schulz, P., *ACS Energy Lett.*, 2018, **3**, 1287-1293.
20 Cherif, F.E., Hamza, M. and Sammouda, H., *J Phys Chem Solids*, 2019, **135**, 109093.
21 Lim, S.S., Giovanni, D., Zhang, Q., Solanki, A., Jamaludin, N.F., Lim, J.W.M., Mathews, N., Mhaisalkar, S., Pshenichnikov, M.S. and Sum, T.C., *Sci. Adv.*, 2019, **5**, eaax3620.
22 Rombach, F. M., Haque, S. A. and Macdonald, T. J., *Energy Environ. Sci.*, 2021, **14**, 5161-5190.
23 Yan, P., Yang, D., Wang, H., Yang, S. and Ge. Z., *Energy Environ. Sci.*, 2022, **15**, 3630–3669.
24 Khan, D., Liu, X., Qu, G., Nath, A.R., Xie, P. and Xu, Z.X., *Small*, 2023, **19**, 2205926.
25 Cheng, Q., Chen, H., Chen, W., Ding, J., Chen, Z., Shen, Y., Wu, X., Wu, Y., Li, Y. and Li, Y., *Angew. Chem. Int. Ed.*, 2023, **62**, e202312231.
26 Yu, X.Y., Gao, D., Li, Z., Sun, X., Li, B., Zhu, Z. and Li, Z., *Angew. Chem. Int. Ed.*, 2023, **62**, e202218752.
27 Fu, Q., Tang, X., Liu, H., Wang, R., Liu, T., Wu, Z., Woo, H.Y., Zhou, T., Wan, X., Chen, Y., et al., *J. Am. Chem. Soc.*, 2022, **144**, 9500-9509.
28 Jeong, M., Yeom, K.M., Kim, S.J., Jung, E.H. and Noh, J.H., *Energy Environ. Sci.*, 2021, **14**, 2419.
29 Wu, X., Gao, D., Sun, X., Zhang, S., Wang, Q., Li, B., Li, Z., Qin, M., Jiang, X., Zhang, C., et al., *Adv. Mater.*, 2023, **35**, 2208431.
30 Yin, X., Song, Z., Li, Z. and Tang, W., *Energy Environ. Sci.*, 2020, **13**, 4057-4086.
31 Dong, L., Hu, Q., Rezaee, E., Chen, Q., Yang, S., Cai, S., Liu, B., Pan, J.H. and Xu, Z.X., *Solar RRL*, 2019, **3**, 1970091.
32 Rakstys, K., Igci, C. and Nazeeruddin, M. K., *Chem. Sci.*, 2019, **10**, 6748-6769.
33 Hu, Q., Rezaee, E., Dong, L., Dong, Q., Shan, H., Chen, Q., Li, M., Cai, S., Wang, L. and Xu, Z.X., *Solar RRL*, 2019, **3**, 1900182.
34 Stecker, C., Liu, Z., Hieulle, J., Zhang, S., Ono, L.K., Wang, G. and Qi, Y., *ACS Nano*, 2021, **15**, 14813-14821.
35 Hu, Q., Rezaee, E., Xu, W., Ramachandran, R., Chen, Q., Xu, H., EL-Assaad, T., McGrath, D.V. and Xu, Z.X., *Small*, 2021, **17**, 2005216.
36 Qu, G., Dong, L., Qiao, Y., Khan, D., Chen, Q., Xie, P., Yu, X., Liu, X., Wang, Y., Chen, J., et al., *Adv. Funct. Mater.*, 2022, **32**, 2206585.
37 Zhai, Y., Wang, K., Zhang, F., Xiao, C., Rose, A.H., Zhu, K. and Beard, M.C., *ACS Energy Lett.*, 2020, **5**, 47-55.
38 Zhang, C., Fan, Y., Huang, X., Zhang, K.H.L., Beard, M.C. and Yang, Y., *J. Chem. Phys.*, 2020, **152**, 144705.
39 Gong, S., Huang, Y., Yu, X., Hu, Q., Liu, J., Meng, J., Wen, Y. and Chen, X., *Cell Rep. Phys. Sci.*, 2023, **4**, 101580.
40 Xue, J., Wang, R., Chen, X., Yao, C., Jin, X., Wang, K.L., Huang, W., Huang, T., Zhao, Y., Zhai, Y., et al., *Science*, 2021, **371**, 636.
41 Fu, J., Xu, Q., Han, G., Wu, B., Huan, C.H.A., Leek, M.L. and Sum, T.C., *Nat. Commun.*, 2017, **8**, 1300.
42 Wang, T., Jin, L., Hidalgo, J., Chu, W., Snaider, J.M., Deng, S., Zhu, T., Lai, B., Prezhdo, O., Correa-Baena, J.P., et al., *Sci. Adv.*, 2020, **6**, eabb1336.
43 Yang, J.P., Meissner, M., Yamaguchi, T., Zhang, X.Y., Ueba, T., Cheng, L.W., Ideta, S., Tanaka, K., Zeng, X.H., Ueno, N., et al., *Solar RRL*, 2018, **2**, 1800132.
44 Poncé, S., Schlipf, M. and Giustino, F., *ACS Energy Lett.*, 2019, **4**, 456-463.
45 Turedi, B., Yeddu, V., Zheng, X., Kim, D.Y., Bakr, O.M. and Saidaminov, M.I., *ACS Energy Lett.*, 2021, **6**, 631-642.
46 Guo, Z., Wan, Y., Yang, M., Snaider, J., Zhu, K. and Huang, L., *Science*, 2017, **356**, 59-62.
47 Zhu, T., Snaider, J.M., Yuan, L. and Huang, L., *Annu. Rev. Phys. Chem.*, 2019, **70**, 219-244.
48 Wagner, L., Schygulla, P., Herterich, J.P., Elshamy, M., Bogachuk, D., Zouhair, S., Mastroianni, S., Wurfel, U., Liu, Y., Zakeeruddin, S.M., et al., *Matter*, 2022, **5**, 2352-2364.
49 Liu, X., Wu, X., Li, B., Cen, Z., Shang, Y., Lian, W., Cao, R., Jia, L., Li, Z., Gao, D., et al., *Energy Environ. Sci.*, 2022, **15**, 4813-4822.
50 Guo, Z., Jena, A.K., Kim, G.M. and Miyasaka, T., *Energy Environ. Sci.*, 2022, **15**, 3171-3222.
51 Zhou, Y., Chen, Y., Zhang, Q., Zhou, Y., Tai, M., Koumoto, K. and Lin, H., *J. Energy Chem.*, 2021, **59**, 730–735.

52 Bi, W., Wu, Y., Chen, C., Zhou, D., Song, Z., Li, D., Chen, G., Dai, Q., Zhu, Y. and Song, H., *ACS Appl. Mater. Interfaces*, 2020, **12**, 24737−24746.
53 Baig, H., Kanda, H., Asiri, A.M., Nazeeruddin, M.K. and Mallick, T., *Sustainable Energy Fuels*, 2020, **4**, 528.
54 Ma, T., An, Y., Li, S., Zhao, Y., Wang, H., Wang, C., Maier, S.A. and Li, X., *ACS Appl. Mater. Interfaces*, 2022, **14**, 29856−29866.
55 Li, X., Zhang, W., Guo, X., Lu, C., Wei, J. and Fang, J., *Science*, 2022, **375**, 434-437.
56 Conradie, J. and Erasmus, E., *J. Electron. Spectrosc. Relat. Phenom.*, 2022, ***259***, 147241.
57 Rand, B.P., Cheyns, D., Vasseur, K., Giebink, N.C., Mothy, S., Yi, Y., Coropceanu, V., Beljonne, D., Cornil, J., Bredas, J.L., et al., *Adv. Funct. Mater.*, 2012, **22**, 2987-2995.
58 Yang, G., Wang, Y.L., Xu, J.J., Lei, H.W., Chen, C., Shan, H.Q., Liu, X.Y., Xu, Z.X. and Fang, G.J., *Nano Energy*, 2017, **31**, 322-330.
59 Zheng, X., Wang, Y., Hu, J., Yang, G., Guo, Z., Xia, J., Xu, Z. and Fang, G., *J. Mater. Chem. A.*, 2017, **5**, 24416.
60 Marcus, R. A., *Annu. Rev. Phys. Chem.*, 1964, **15**, 155-196.
61 Marcus, R. A., *J. Chem. Phys.*, 1956, **24**, 966-978.
62 Yang, Y., Yang, M., Moore, D.T., Yan, Y., Miller, E.M., Zhu, K. and Beard, M.C, *Nat. Energy*, 2017, **2**, 16207.